Role of ^{99m}Tc-Octreotide Acetate Scintigraphy in Suspected Lung Cancer Compared with ^{18}F-FDG Dual-Head Coincidence Imaging

Feng Wang[1], Zizheng Wang[1], Weixuan Yao[1], Hong Xie[2], Jie Xu[1], and Li Tian[3]

[1]Department of Nuclear Medicine, Nanjing First Hospital, Nanjing Medical University, Nanjing, China; [2]Respiratory Department, Nanjing First Hospital, Nanjing Medical University, Nanjing, China; and [3]Respiratory Department, Nanjing Chest Hospital, Nanjing, China

The aim of this study was to evaluate the clinical value of tomographic ^{99m}Tc-octreotide acetate (hereafter, ^{99m}Tc-octreotide) scintigraphy in the detection of patients with suspected lung cancer in comparison with that of ^{18}F-FDG dual-head coincidence imaging (DHC). **Methods:** Forty-four consecutive patients with suspected pulmonary neoplasms underwent tomographic ^{99m}Tc-octreotide scintigraphy and ^{18}F-FDG coincidence imaging using the same gantry. The region of interest was drawn on the entire primary lesion. The tumor-to-normal tissue tracer values for both ^{99m}Tc-octreotide and ^{18}F-FDG were determined using region of interests and expressed as T/N_r and T/N_m, respectively. Final diagnosis was confirmed by histopathologic analysis or clinical follow-up. **Results:** Thirty-one of the 44 patients had lung cancer—6 with small cell lung cancer (SCLC) and 25 with non–small cell lung cancer (NSCLC). Thirteen of the 44 patients had benign lung lesions. The sensitivity, specificity, positive predictive value, and negative predictive value of ^{99m}Tc-octreotide were 100%, 75.7%, 90.1%, and 100%, respectively, and of ^{18}F-FDG DHC were 100%, 46.1%, 83.8%, and 100%, respectively. In the 31 patients with malignant tumors, all 38 abnormal lymph nodes in 20 patients showed abnormal high focal uptake of ^{18}F-FDG; only 7 patients with 10 regional lymph adenopathies showed moderate uptake of ^{99m}Tc-octreotide. Thirteen patients with 39 distant sites of abnormal uptake visualized (imaging stage IV) with ^{99m}Tc-octreotide included 2 patients with brain metastases, 6 patients with pleural invasion and multiple bone metastasis, 2 patients with contralateral internal lung metastasis and pleural invasion, and 3 patients with only multiple bone metastasis. The final diagnosis was confirmed by histopathology or clinical follow-up. **Conclusion:** The sensitivity of ^{99m}Tc-octreotide for the detection of lung cancer at the primary lesion was comparable with that of ^{18}F-FDG coincidence imaging. Tomographic ^{99m}Tc-octreotide scintigraphy had lower sensitivity for the detection of hilar and mediastinal lymph node metastasis compared with that of ^{18}F-FDG coincidence PET, but it had high sensitivity for the detection of remote metastatic lesions. However, because of the small population, further investigation is necessary.

Received Feb. 12, 2007; revision accepted May 31, 2007.

For correspondence or reprints contact: Zizheng Wang, MD, Department of Nuclear Medicine, Nanjing First Hospital, Nanjing Medical University, 68 Changle Rd., Nanjing, China, 210006.

E-mail: zzwang136@yahoo.com.on

Key Words: lung cancer; scintigraphy; somatostatin receptor scintigraphy; ^{18}F FDG; dual-head coincidence imaging

J Nucl Med 2007; 48:1442–1448
DOI: 10.2967/jnumed.107.040824

Lung cancer is the leading cause of cancer death in both developed and developing countries, including China (*1,2*). The overall 5-y survival rate in patients with lung cancers after treatment is about 15% (*1,3*). Two thirds of patients with non–small cell lung cancer (NSCLC), which accounts for 80% of lung cancers, were diagnosed at the unresectable advanced stage (*4,5*).

The conventional noninvasive diagnostic modalities currently used in evaluating lung tumors—chest x-ray, CT, and sputum cytology—have a high percentage of indeterminate diagnosis (*6,7*). ^{18}F-FDG PET and PET/CT have been widely studied in the detection of lung cancers for diagnosis, staging, and restaging (*8–16*). However, in developing countries, the high cost of this equipment and the lack of general availability have limited their widespread clinical use.

The affinity of receptor analogs such as somatostatin (SST) in some malignant lung tumors has been demonstrated (*17–20*). The aim of this study was to determine the efficacy of the SST receptor ([SSTR] octreotide acetate; hereafter, octreotide) imaging in diagnosing patients with suspected lung cancer in comparison with that of ^{18}F-FDG coincidence imaging in the same consecutive 44 patients.

MATERIALS AND METHODS

Patients

The Institutional Review Board of the Nanjing Medical University as well as the local ethics committee approved this investigation. Written consent was obtained from all patients. Forty-four consecutive patients with suspected lung cancer (13 women, 31 men; age range, 44–83 y; average age, 62 ± 10 y [mean ± SD]) were prospectively enrolled in this study. Conventional methods, such as plain chest x-ray and chest CT were performed on all patients, who either refused or could not endure an invasive technique such as bronchoscopy or transthoracic biopsy. All patients underwent

^{99m}Tc-octreotide scintigraphy and ^{18}F-FDG coincidence imaging. The final diagnosis and stage were confirmed by histopathologic findings or clinical follow-up.

^{99m}Tc-Octreotide Image Acquisition and Interpretation

Ten micrograms of octreotide (Sandostatin; Novartis Pharma Schweiz AG) were labeled with ^{99m}Tc-pertechnetate in a 1-mL volume. The mean radiochemical purity ± SD was 95.1% ± 2.9%. ^{99m}Tc-Octreotide (1,110 MBq [30 mCi]) was administrated intravenously, and planar whole-body static images were acquired about 4 h later. Immediately thereafter, SPECT/CT images of the chest and the upper abdomen, including the adrenal glands (Millennium VG, Hawkeye; GE Healthcare), were obtained. SPECT data were acquired in a 128 × 128 matrix through 360° rotation with 64 projections. The acquisition time for each projection was 40 s. Transverse slices were reconstructed with an ordered-subset expectation maximization (OSEM) iterative algorithm and formatted as a 128 × 128 matrix. The CT images were used for attenuation correction of the SPECT image datasets and for better anatomic delineation of the SPECT images.

The SPECT/CT images of the thorax and upper abdomen were displayed in the 3 orthogonal planes on the camera workstation and

TABLE 1
Clinical Information and Histopathologic Database Used in Study

Patient no.	Sex	Age (y)	Histology	Primary lesion (cm)	Staging	T/N_r	T/N_m
1	F	52	Adenocarcinoma	2.0	T1 N3	2.54	5.56
2	M	51	Squamous cell carcinoma	4.2	T2 N3	2.24	6.62
3	M	57	Squamous cell carcinoma	3.0	T2 N0	4.1	9.86
4	M	75	Adenosquamous carcinoma	4.8	T4 N0	3.91	7.34
5	F	55	Adenocarcinoma	3.6	T2 N3 M1	3.29	5.46
6	M	59	Adenocarcinoma	4.2	T3 N3	2.82	6.35
7	M	76	Undifferentiated lung cancer	11.0	T4 N3	5.58	10.56
8	M	72	Adenocarcinoma	3.8	T2 N1	2.30	5.32
9	F	65	Adenocarcinoma	5.2	T4 N3 M1	3.78	8.23
10	F	61	Squamous cell carcinoma	3.2	T2 N0 M1	4.06	7.16
11	M	42	Squamous cell carcinoma	6.2	T4 N3 M1	4.61	5.35
12	M	70	Squamous cell carcinoma	7.8	T4 N3	3.36	10.23
13	F	60	Squamous cell carcinoma	5.3	T2 N3	2.98	9.18
14	M	71	Squamous cell carcinoma	3.5	T2 N2	3.63	6.45
15	M	75	Adenocarcinoma	4.8	T4 N3 M1	2.57	4.12
16	M	70	Squamous cell carcinoma	8.5	T4 N3	3.59	5.36
17	F	63	Adenocarcinoma	3.5	T2	3.87	4.96
18	M	64	Adenocarcinoma	4.5	T2 N3 M1	2.68	5.09
19	M	64	Small-cell lung carcinoma	6.5	T3 N2	3.42	4.49
20	F	64	Adenocarcinoma	3.8	T2 N3 M1	2.62	5.54
21	M	60	Adenocarcinoma	7.1	T3 N2	2.68	5.31
22	M	71	Adenocarcinoma	4.5	T2 N3 M1	4.13	6.23
23	F	44	Small-cell lung carcinoma	5.0	T3 N3 M1	3.32	5.16
24	M	70	Squamous cell carcinoma	8.5	T4 N3	3.36	7.16
25	M	73	Adenocarcinoma	5.1	T2 N0	2.89	4.86
26	M	54	Squamous cell carcinoma	7.5	T4 N3 M1	3.46	8.19
27	M	76	Adenocarcinoma	3.2	T4 N0	3.78	4.61
28	M	51	Small-cell lung carcinoma	7.1	T4 N3 M1	3.63	5.34
29	M	75	Small-cell lung carcinoma	2.8, 5.6	T4 N0 M1	3.98	4.55
30	F	56	Small-cell lung carcinoma	2.0, 5.0	T2 N0 M1	3.68	3.99
31	F	39	Small-cell lung carcinoma	3.2	T4 N0	4.09	5.32
32	F	51	Fibroma	1.2	—	1.29	1.42
33	F	66	Tuberculosis	3.3	—	1.13	2.10
34	F	70	Granuloma	2.3	—	1.56	3.92
35	F	62	Hamartoma	1.6	—	1.49	2.13
36	M	62	Tuberculosis	1.2	—	1.36	3.88
37	M	83	Pneumonia	2.5	—	1.78	1.89
38	M	75	Interstitial pneumonitis	1.0	—	1.39	1.78
39	M	46	Clear cell tumor	2.5	—	1.24	4.12
40	M	75	Tuberculosis	4.0	—	1.35	3.89
41	M	30	Tuberculosis	1.5	—	4.69	6.93
42	M	71	Granuloma	2.5	—	1.59	1.89
43	M	68	Tuberculosis	2.6	—	3.68	4.96
44	M	50	Tuberculosis	3.0	—	3.89	5.69

TNM staging was determined by histopathology or other imaging modalities. Tumor-to-normal tissue uptake ratios of ^{18}F-FDG DHC are expressed as T/N_m. Tumor-to-normal tissue uptake ratios of ^{99m}Tc-octreotide imaging are expressed as T/N_r.

were interpreted separately and independently by 3 nuclear medicine physicians who were unaware of the clinical diagnosis and the results of other imaging tests. Focal areas of increased tracer uptake compared with adjacent lung tissue activity were considered positive for malignancy. Lesions with radiotracer uptake less than or equal to adjacent or surrounding lung tissue activity were interpreted as benign. Hilar and mediastinal foci with activity greater than the adjacent mediastinal tissue were interpreted as abnormal lymph adenopathy. Regions of interest (ROIs) were drawn on the entire primary lesion and the contralateral normal lung tissue; tumor uptake of ^{99m}Tc-octreotide activity was estimated by using ROIs that were drawn around the primary lesions, and tumor-to-normal tissue activity (T/N_r) ratios were generated.

^{18}F-FDG Coincidence Image Acquisition and Image Interpretation

One day after tomographic ^{99m}Tc-octreotide imaging, ^{18}F-FDG dual-head coincidence imaging (DHC) was performed 60 min after intravenous injection of ^{18}F-FDG (296–370 MBq). Each patient had fasted for at least 6 h prior to the injection. Emission data were acquired for 10 rotations of 360° in 1.8 min per revolution using hybrid SPECT/CT with a coincidence system (Millennium VG, Hawkeye; GE Healthcare). Images from the base of the skull to the pelvic floor were acquired with 2 separate tomographic examinations. Brain images were acquired separately. Low-dose CT (2.5 mA) was acquired for 40 revolutions of 360° in 15 s per revolution for attenuation correction and image fusion. Data were reconstructed with an ordered-subset expectation maximization (OSEM) iterative algorithm. Functional, anatomic, and fusion images were obtained; all images were formatted to a 128 × 128 matrix. The ^{18}F-FDG images were displayed in the 3 orthogonal planes on the camera workstation.

Images were analyzed visually by the same 3 experienced nuclear medicine physicians who had analyzed the ^{99m}Tc-octreotide images and were unaware of the final clinical diagnosis. Interpretation was based on attenuation-corrected images. Any focal activity in a known lesion with an intensity higher than the normal mediastinal activity was considered malignant. Any hilar or mediastinal focal increased activity greater than that of the surrounding mediastinal activity was regarded as a metastatic lymph node. Any focal distant increased activity that did not correspond to a normal physiologic structure and had increased intensity was considered as a metastatic lesion. Tumor-to-normal tissue uptake ratios of ^{18}F-FDG were also calculated for the primary lesion (T/N_m).

Statistical Analysis

The data were analyzed and presented as the mean ± SD. The sensitivity, specificity, negative predictive value (NPV), and positive predictive value (PPV) were estimated for ^{99m}Tc-octreotide and ^{18}F-FDG images using SPSS software, version 10.0. The McNemar test was used to assess the ^{18}F-FDG coincidence PET images. The efficacy of tomographic ^{99m}Tc-octreotide for differentiation of lung cancer from benign lesions was determined with the Student t test.

RESULTS

The demographics, histopathology, and staging of the patients are provided in Table 1.

Primary Lung Lesion

Of the consecutive 44 patients, 31 (70.5%) had malignant neoplasms identified by histopathologic findings—6 patients with small-cell lung cancer (SCLC) and 25 patients with NSCLC. Thirteen of the 44 patients had benign lesions (Table 1). Tissues for histopathology were obtained by thoracic surgery in 18 patients, with fine-needle aspiration in 12 patients, and during bronchoscopy in 8 patients. The benign nature of the lesions was confirmed on clinical follow-up in 6 patients. One patient with a benign clear cell tumor showed a high uptake of ^{18}F-FDG but no obvious uptake of ^{99m}Tc-octreotide (Fig. 1). Pleural invasions in 2 patients were clearly visualized on ^{99m}Tc-octreotide and ^{18}F-FDG images (Figs. 2 and 3).

The median size of the lesions (average of the 2 longest dimensions on the chest CT) was 4.8 cm (range, 1.0–11.0 cm).

PPVs and NPVs of ^{99m}Tc-octreotide scintigraphy and ^{18}F FDG coincidence imaging for the diagnosis of primary lesions are shown in Table 2. The sensitivity and specificity of the detection of primary lesions were not statistically significant between these 2 imaging modalities ($\chi^2 = 0.72$; $P = 0.395$).

The T/N_r for octreotide was 3.03 ± 1.09, and the T/N_m for FDG was 5.51 ± 2.13. The ^{99m}Tc-octreotide tumor uptake correlated with that of ^{18}F-FDG uptake ($r = 0.66$; $P < 0.0001$). The uptake of ^{99m}Tc-octreotide in benign lesions was 2.03 ± 1.02 and was significantly less than that for malignancy (3.45 ± 0.73; $t = 4.82$; $P < 0.001$).

Metastatic Lymph Adenopathy

The staging status and clinical information in the 31 patients with histopathologically documented lung cancer are shown in Table 3. In 20 patients, all of the 38 regional lymph node metastatic lesions showed a high degree of ^{18}F-FDG uptake. However, only 7 of those 20 patients with metastatic lymph node adenopathy were detected on ^{99m}Tc-octreotide scintigraphy. The sensitivity of ^{99m}Tc-octreotide for the detection of lymph node metastases was low—35% compared with ^{18}F-FDG coincidence imaging (100%).

Distant Metastatic Lesions

There were 39 distant metastatic sites in 13 patients, which were visualized by both ^{99m}Tc-octreotide tomography and

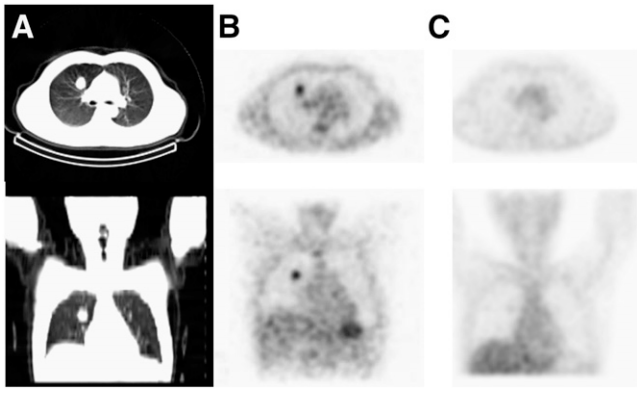

FIGURE 1. A 46-y-old male patient with benign clear cell tumor. (A) CT scans showed abnormality in right upper lobe. (B) ^{18}F-FDG coincidence images had intense uptake in lesion. (C) ^{99m}Tc-Octreotide images were negative in lesion.

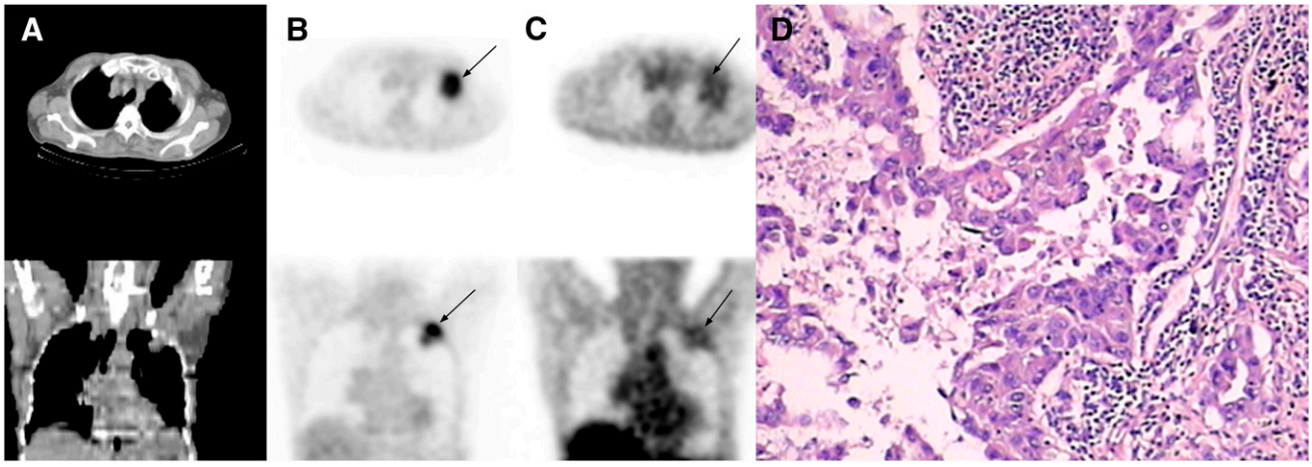

FIGURE 2. A 75-y-old male patient with adenosquamous lung cancer in left upper lobe. (A) CT scans showed abnormality in left upper lobe. (B) ^{18}F-FDG coincidence images had intense uptake in lesion (arrows). (C) ^{99m}Tc-Octreotide images showed intense uptake in primary tumor and pleura (arrows). (D) Adenosquamous lung cancer and pleural invasion were verified on histology.

^{18}F-FDG coincidence imaging. Two patients had brain metastases, 6 patients had pleural invasion and multiple bone metastases, 2 patients had contralateral internal lung metastases and pleural invasion, and 3 patients had only multiple bone metastases. The 2 patients with brain metastases had intense uptake of ^{99m}Tc-octreotide: 1 patient showed decreased uptake of ^{18}F-FDG, as demonstrated in Fig. 4, whereas the other patient showed intense focal uptake of ^{18}F-FDG. Both patients had a high accumulation of ^{99m}Tc-octreotide (Fig. 4). All of these metastatic lesions were confirmed by histopathology or other noninvasive imaging modalities such as bone scan, CT, and MRI.

DISCUSSION

Conventional noninvasive imaging modalities, such as plain chest x-ray and CT, continue to play an important role in the detection of lung cancer but often fail to distinguish between malignant and benign lung tumors (*21*). Definitive diagnosis and staging have traditionally depended on more invasive techniques. However, even these invasive procedures—such as bronchoscopy and transbronchial or transthoracic biopsy—may fail to provide a conclusive diagnosis (*22,23*), despite their known potential complications (*24*).

SST and synthesized longer-acting analogs such as octreotide and lanteotide have many predominantly inhibitory hormonal functions on the gastrointestinal tract and nervous system as well as direct and indirect antineoplastic effects. SSTRs are integral membrane glycoproteins that are distributed in a variety of tissues. Five subtypes have been identified and cloned. Alteration of SSTR expression during disease states—such as their overexpression in many neoplasia—can be exploited by imaging techniques (*18,25,26*). SSTR scintigraphy with ^{111}In-labeled SST analogs has been well documented, especially in neuroendocrine tumors (*26–28*).

The fact that SSTRs are overexpressed in many malignant tumors provides the basis for differentiating malignant tissues from other tissues by nuclear imaging using SSTR-binding radiotracers. Several reports have confirmed the

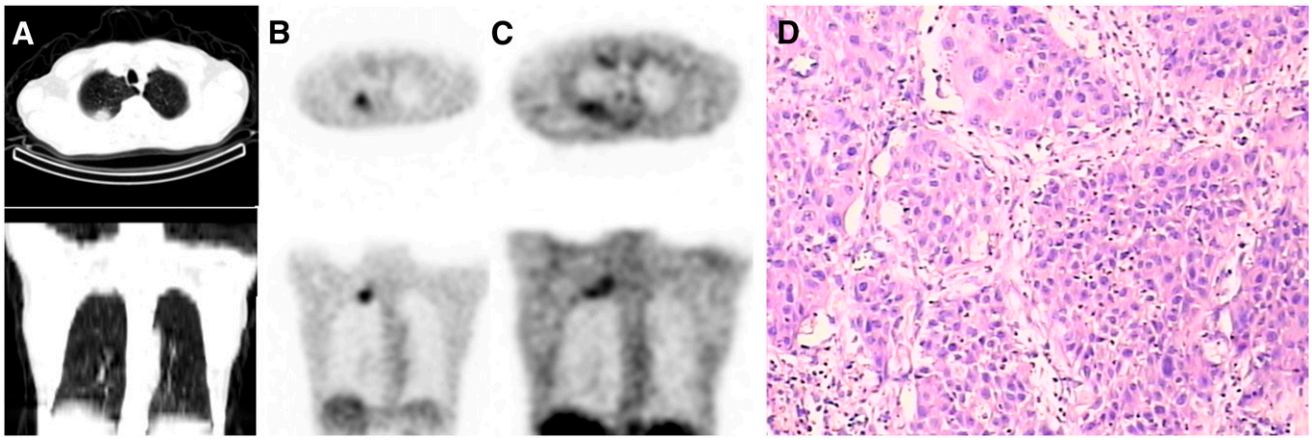

FIGURE 3. A 57-y-old male patient with squamous lung cancer. (A) CT scans showed neoplasm high in upper lobe of right lung. (B) ^{18}F-FDG coincidence images had focal uptake in lesion. (C) ^{99m}Tc-Octreotide images had focal high uptake in lesion. (D) Squamous lung cancer and pleura and rib invasion were verified on histology.

TABLE 2
Efficacy of ^{99m}Tc-Octreotide for Detection of Primary Lesion and Lymph Node Involvement Compared with ^{18}F-FDG

	^{18}F-FDG DHC				^{99m}Tc-Octreotide			
Lesion location	Sensitivity (%)	Specificity (%)	PPV (%)	NPV (%)	Sensitivity (%)	Specificity (%)	PPV (%)	NPV (%)
Primary lesion	100 (31–31)	46.1 (6–13)	83.8 (31–38)	100 (6–6)	100 (31–31)	75.7 (9–13)	90.1 (31–35)	100 (9–9)
Metastatic hilar or mediastinal LN	100 (20–20)	100 (11–11)	100 (20–20)	100 (11–11)	35 (7–20)	100 (7–7)	100 (7–7)	46 (11–24)

LN = lymph node.
Data are expressed as percentage, with range in parentheses.

presence of SSTRs on NSCLC tumors and cell lines (*29–31*). Other studies have shown that SST analog scintigraphy labeled with ^{111}In- and ^{99m}Tc-pertechnetate can be used for the detection of solitary pulmonary nodules (*19,20,32*). ^{99m}Tc-Depreotide (NeoTect; Berlex Laboratories) is one example.

Octreotide is also a synthetic analog of SST, which is available in most hospitals. A 1-step labeling reaction, without additional purification, results in a high, stable radiochemical yield with ^{99m}Tc-pertechnetate (^{99m}Tc-octreotide); the radiochemical purity was >98%. No complications or side effects were observed, and the labeling method is very simple.

In this study, 44 clinically indeterminate patients with lung neoplasms were enrolled, and the clinical value of ^{99m}Tc-octreotide scintigraphy in the detection of lung cancer was evaluated and compared with that of ^{18}F-FDG DHC.

Our results demonstrated that ^{99m}Tc-octreotide scintigraphy is a sensitive test for the detection of primary lung cancer, as reported previously (*32,33*). The sensitivity of tomographic ^{99m}Tc-octreotide scintigraphy for the detection of primary lung cancer is similar to that of ^{18}F-FDG coincidence imaging. However, the specificity and the PPVs of tomographic ^{99m}Tc-octreotide scintigraphy are higher than those of ^{18}F-FDG coincidence PET. Despite the high sensitivity of ^{18}F-FDG PET, false-positive findings—such as in patients with inflammatory processes—might hamper proper patient management (*34*). ^{99m}Tc-Octreotide scintigraphy does not seem to be affected as much by inflammatory processes. In our study, 1 patient with a benign clear cell tumor, 2 patients with granulomas, and another patient with tuberculosis showed no focal accumulation of ^{99m}Tc-octreotide, despite the presence of high focal ^{18}F-FDG activity. Only half of the patients with tuberculosis (3/6) showed increased activity on ^{99m}Tc-octreotide scans. One might consider the combined use of these 2 radionuclides to decrease the false-positive rate of ^{18}F-FDG scans. However, the discrepancy between these 2 diagnostic techniques could not be evaluated further because no patient with a carcinoid tumor was found in this relatively small group.

TABLE 3
Demographic and Clinical Staging of Study Population

Parameter	Value
No. of patients	44
Age range (y)	39–83
Women/men	12/32
Benign/malignant lesions	13/31
Surgery/biopsy/bronchoscopy/clinicoradiology	18/12/8/6
Lymph node adenopathy/no lymph node adenopathy	20/11
Clinical T factor for malignant lesions (1/2/3/4)	1/10/3/17
Clinical N status (0/1/2/3)	11/1/3/16
Distant metastasis/no distant metastasis	13/18
Contralateral lung intrametastasis/no lung intrametastasis	2/29
Pleural invasion/no pleural invasion	8/23
Bone metastasis/no bone metastasis	9/22
Brain metastasis/no brain metastasis	2/29

With respect to metastatic hilar and mediastinal nodes, a large meta-analysis indicated that ^{18}F-FDG PET is a relatively accurate method for assessing the status of the mediastinal lymph node regions (*35*). Our results revealed that ^{18}F-FDG coincidence imaging was more accurate than ^{99m}Tc-octreotide scintigraphy for the detection of mediastinal and hilar lymph node involvement. For example, all 20 patients with a total of 38 hilar and mediastinal metastatic lymph nodes had increased ^{18}F-FDG activity in their lesions on ^{18}F-FDG coincidence images. However, only 7 patients with 10 of the hilar and mediastinal nodes had mild-to-moderate ^{99m}Tc-octreotide uptake; the sensitivity for the detection of hilar and mediastinal lymph node metastasis was 35%, significantly lower than that for ^{18}F-FDG coincidence imaging. This low sensitivity was due to the relatively high background of ^{99m}Tc-octreotide in the mediastinum and hilum of lung compared with that of ^{18}F-FDG.

On the other hand, the sensitivity of ^{99m}Tc-octreotide scintigraphy for the detection of remote metastatic lesions was high. Thirty-nine distant metastatic sites in 13 patients were visualized by both ^{99m}Tc-octreotide and ^{18}F-FDG imaging. These 13 patients included 2 with brain metastasis, 6 with pleural invasion and multiple bone metastasis, 2 with contralateral internal lung metastasis and pleural invasion, and 3 with only multiple bone metastasis. Other

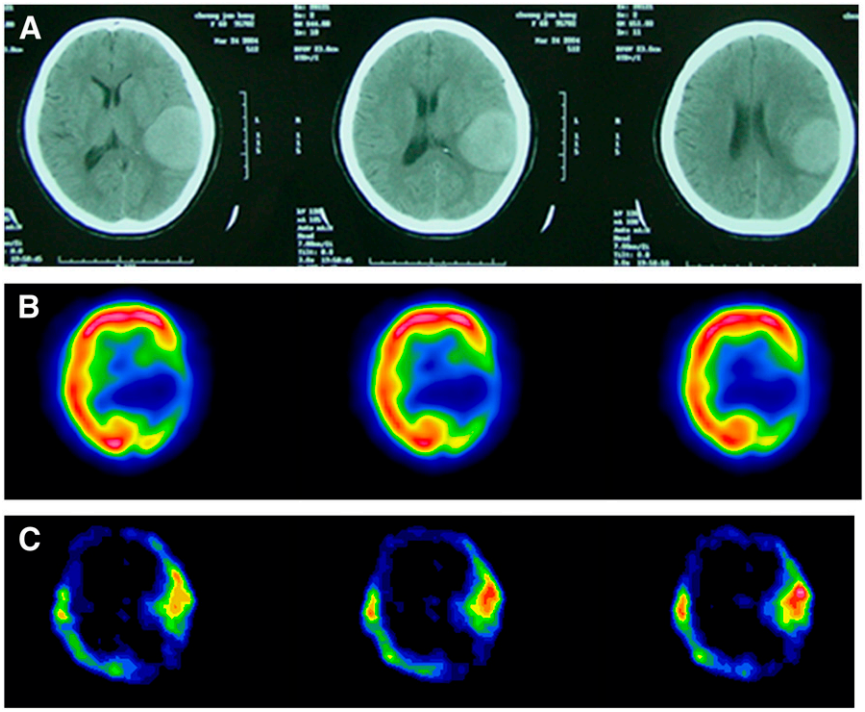

FIGURE 4. A 65-y-old woman with lung adenocarcinoma. (A) CT scans revealed brain metastasis and peripheral edema in left temporal lobe. (B) ^{18}F-FDG images showed low uptake in brain lesion. (C) ^{99m}Tc-Octreotide images showed focal uptake in brain lesion.

trials have reported that ^{18}F-FDG PET could detect unexpected distant metastasis in approximately 13% of patients, which had a large impact on patient management (*36,37*). Our study suggested that ^{99m}Tc-octreotide scintigraphy was also valuable for the detection of distant metastatic disease, which led to further diagnostic investigation.

In the present study, we also noted that the resolution of the instrument used was limited compared with that of dedicated PET/CT. However, most patients were in advanced stages of disease, and the size of the primary lesion was relatively large in this study, which might have resulted in a high sensitivity of ^{99m}Tc-octreotide and ^{18}F-FDG in the detection of the primary lesion.

This prospective study confirmed that ^{99m}Tc-octreotide tomography had a high sensitivity for the detection of the primary lesion and distant metastasis in patients with suspected lung cancer, whereas it had a low sensitivity for the detection of mediastinal and hilar lymph node metastasis. However, ^{99m}Tc-octreotide tomography might be an alternative method for the diagnosis of lung cancer, especially in developing countries, where the availability of PET/CT or dedicated PET is limited because of the high cost.

CONCLUSION

Tomographic ^{99m}Tc-octreotide scintigraphy is an effective noninvasive technique for diagnosing lung cancer, especially for the detection of primary lesions. Its sensitivity and specificity for the primary lesions are comparable to those of ^{18}F FDG coincidence imaging. Although ^{99m}Tc-octreotide has a high sensitivity for the detection of remote metastatic lesions, it has a lower sensitivity for the detection of hilar and mediastinal lymph node metastasis. Further investigation is needed to confirm the results of this relatively small population study.

ACKNOWLEDGMENTS

We are grateful to Dr. Xiu-Jie Liu (Cardiovascular Institute and Fu Wai Hospital, Beijing, China) for valuable advice and assistance in revision of this article. This research was supported by Jiangsu Government Science grant BS2004507 and Nanjing Health Bureau grant zx0214, China.

REFERENCES

1. Jemal A, Thomas A, Murray T, et al. Cancer statistics: 2002. *CA Cancer J Clin.* 2002;52:23–47.
2. Xiong J-F, Zhou H-B, Chi H-S, et al. Epidemic trend study of malignant tumors incidence from 1999 to 2004 in Shenzhen. *Chin J Cancer Prev Treat.* 2006;13:572–576.
3. Yang L, Li L, Chen Y, et al. Mortality time trends and the incidence and mortality estimation and projection for lung cancer in China. *Chin J Lung Cancer.* 2005;8:274–278.
4. Zhang S-W, Chen W-Q, Kong L-Z, et al. An analysis of cancer incidence and mortality from 30 cancer registries in China, 1998–2002. *Bull Chin Cancer.* 2005;15:430–448.
5. Lee C, Kang KH, Koh Y, et al. Characteristics of lung cancer in Korea, 1997. *Lung Cancer.* 2000;30:15–22.
6. Deslauriers J, Gregoire J. Clinical and surgical staging of non-small cell lung cancer. *Chest.* 2000;117(4 suppl 1):96S–103S.
7. Webb WR, Gatsouris S, Zerhouni EA, et al. CT and MR imaging in staging non-small cell bronchogenic carcinoma: report of the Radiology Diagnostic Oncology Group. *Radiology.* 1992;182:319–323.
8. Gupta NC, Maloof J, Gunel E. Probability of malignancy in solitary pulmonary nodules using fluorine-18-FDG and PET. *J Nucl Med.* 1996;37:943–948.
9. Dewan NA, Shehan CJ, Reeb SD, Gobar LS, Scott WJ, Ryschon K. Likelihood of malignancy in a solitary pulmonary nodule. *Chest.* 1997;112:416–422.
10. Herder GJ, Golding RP, Gobar L, et al. The performance of 18-F-fluorodeoxyglucose positron emission tomography in small solitary pulmonary nodules. *Eur J Nucl Med Mol Imaging.* 2004;31:1231–1236.

11. Lowe VJ, Fletcher JW, et al. Prospective investigation of positron emission tomography in lung nodules. *J Clin Oncol.* 1998;16:1075–1084.
12. Van Tinteren H, Hoekstra OS, Smit EF, et al. Effectiveness of positron emission tomography in the preoperative assessment of patients with suspected nonsmall-cell lung cancer: the PLUS multicentre randomised trial. *Lancet.* 2002;359: 1388–1392.
13. Pieterman RM, van Putten JWG, Meuzelaar JJ, et al. Preoperative staging of non-small cell lung cancer with positron emission tomography. *N Eng J Med.* 2000;343:254–261.
14. Port JL, Kent MS, Korst RJ, et al. Positron emission tomography scanning poorly predicts response to preoperative chemotherapy in non-small cell lung cancer. *Ann Thorac Surg.* 2004;77:254–259.
15. Akhurst T, Downey RJ, Ginsberg MS, et al. An initial experience with FDG PET in the imaging of residual disease after induction therapy for lung cancer. *Ann Thorac Surg.* 2002;73:259–266.
16. Choi NC, Fischman AJ, Niemierko A, et al. Dose-response relationship between probability of pathologic tumor control and glucose metabolic rate measured with FDG PET after preoperative chemoradiotherapy in locally advanced non-small-cell lung cancer. *Int J Radiat Oncol Biol Phys.* 2002;54:1024–1035.
17. Kwekkeboom DJ, Kho GS, Lamberts SW, et al. The value of octreotide scintigraphy in patients with lung cancer. *Eur J Nucl Med.* 1994;221:1106–1113.
18. O'Byrne KJ, Carney D. Somatostatin and the lung. *Lung Cancer.* 1993;10: 151–172.
19. Blum J, Handmaker H, Rinne N, et al. The utility of a somatostatin-type receptor binding peptide radiopharmaceutical (P829) in the evaluation of solitary pulmonary nodules. *Chest.* 1999;115:224–232.
20. Blum J, Handmaker H, Lister-James J, et al. A multicenter trial with a somatostatin analog ^{99m}Tc depreotide in the evaluation of solitary pulmonary nodules. *Chest.* 2000;117:1232–1237.
21. Erasmus JJ, McAdams HP, Connolly JE. Solitary pulmonary nodules. Part II. Evaluation of the indeterminate nodule. *Radiographics.* 2000;20:59–66.
22. Salathe M, Soler M, Bolliger CT, et al. Transbronchial needle aspiration in routine fiberoptic bronchoscopy. *Respiration.* 1992;59:5–8.
23. Schenk DA, Bower JH, Bryan CL, et al. Transbronchial needle aspiration staging of bronchogenic carcinoma. *Am Rev Respir Dis.* 1986;134:146–148.
24. Kazerooni EA, Lim FT, Mikhail A, et al. Risk of pneumothorax in CT-guided transthoracic needle aspiration biopsy of the lung. *Radiology.* 1996;198:371–375.
25. Reubi JC. Neuropeptide receptors in health and disease: the molecular basis for in vivo imaging. *J Nucl Med.* 1995;36:1825–1835.
26. Virgolini I, Pangerl T, Bischof C, et al. Somatostatin receptor expression in human tissues: a prediction for diagnosis and treatment of cancer. *Eur J Nucl Med.* 1993;20:716–731.
27. Legovini P, Demis E, Billeci D, et al. 111Indium-pentetrotide pituitary scintigraphy and hormonal responses to octretide in acromegalic patients. *J Endocrinol Invest.* 1997;20:424–428.
28. De Kerviler E, Cardiot G, Lebtahi R, et al. Somatostatin receptor in forty eight patients with the Zollinger-Ellison syndrome. *Eur J Nucl Med.* 1994;21:1191–1197.
29. Reubi JC, Laissue J, Krenning EP, Lamberts SWJ. Somatostatin receptors in human cancer: incidence, characteristics, functional correlates and clinical application. *J Steroid Biochem Mol Biol.* 1992;43:27–35.
30. O'Byrne KJ, Carney DN. Somatostatin and the lung. *Lung Cancer.* 1993;10: 151–172.
31. Virgolini I, Leimer M, Handmaker H, et al. Somatostatin receptor subtype specificity and in vitro binding of a novel tumour tracer, ^{99m}Tc-P829. *Cancer Res.* 1998;58:1850–1859.
32. Grewal RK, Dadparvar S, Yu JQ, et al. Efficacy of Tc-99m depreotide scintigraphy in the evaluation of solitary pulmonary nodules. *Cancer J.* 2002;8: 400–404.
33. Kahn D, Menda Y, Kernstine K, et al. The utility of ^{99m}Tc depreotide compared with F-18 fluorodeoxyglucose positron emission tomography and surgical staging in patients with suspected non-small cell lung cancer. *Chest.* 2004;125: 494–501.
34. Shreve PD, Anzai Y. Wahl RL. Pitfalls in oncologic diagnosis with FDG-PET imaging: physiologic and benign variants. *Radiographics.* 1999;19:61–67.
35. Dwamena BA, Sonnad SS, Angobaldo JO, et al. Metastases from non-small cell lung cancer: mediastinal staging in the 1990s—meta-analytic comparison of PET and CT. *Radiology.* 1999;213:530–536.
36. Baum RP, Hellwig D, Mezzetti M. Position of nuclear medicine modalities in the diagnostic workup of cancer patients: lung cancer. *Q J Nucl Med Mol Imaging.* 2004;48:119–142.
37. MacManus MP, Hicks RJ, Matthews JP, et al. High rate of detection of unsuspected distant metastases by PET in apparent stage III non-small-cell lung cancer: implications for radical radiation therapy. *Int J Radiat Oncol Biol Phys.* 2001;50:287–293.